Clast imbrications in coarse-grained mountainous streams and stratigraphic archives possibly suggest deposition under upper flow regime conditions

Fritz Schlunegger, Philippos Garefalakis
Institute of Geological Sciences
University of Bern, Switzerland
fritz.schlunegger@geo.unibe.ch
philippos.garefalakis@geo.unibe.ch

Abstract

Clast imbrications are one of the most conspicuous sedimentary structures in coarse-grained clastic deposits of modern rivers but also in the stratigraphic record. In this paper, we test whether the formation of such a fabric could be related to the occurrence of upper flow regime conditions in streams. To this extent, we calculated the Froude number at the incipient motion of coarse-grained bedload for various values of relative bed roughness and stream gradient as these are the first order variables that can particularly be extracted from stratigraphic records. We found that a steeper energy gradient, or slope, and a larger bed roughness tend to favor the occurrence of supercritical flows. We also found that at the incipient motion of grains, the ratio ϕ between the critical shear stress for the entrainment of a sediment particle and its inertial force critically controls whether flows tend to be super- or subcritical during sediment entrainment. We then mapped the occurrence of clast imbrications in Swiss streams and compared these data with the outcomes of the hydrologic calculations. The results reveal that imbrications possibly record supercritical flows provided that (i) ϕ–values are larger than c. 0.05, which might be appropriate for streams in the Swiss Alps; (ii) average stream gradients exceed c. 0.5±0.1°; and that (iii) relative bed roughness values, i.e. the ratio between the water depth d and the D_{84}, are larger than ~0.06±0.01. While we cannot rule out that imbrication may be formed during subcritical flows with ϕ–values as low as 0.03, as a large number of flume experiments reveal, our results from Alpine streams suggest that clast imbrications are likely recorders of upper flow regime conditions, provided that the clasts form well-sorted and densely packed clusters. We consider that these differences may be rooted in a misfit between the observational and experimental scales.

1 Introduction

Conglomerates, representing the coarse-grained spectrum of clastic sediments, bear key information about the provenance of the material (Matter, 1964), the environment in which these sediments were deposited (Rust, 1978; Middleton and Trujillo, 1984), and the hydro-climatic conditions upon transport and deposition of the sediments (Duller et al., 2012; D'Arcy et al., 2017). Conglomerates display the entire range of possible sedimentary structures including a massive-bedded fabric, cross-beds and horizontal stratifications. However, the most striking features are clast imbrications (Figure 1A), which refer to a depositional fabric where sediment particles of similar sizes overlap each other, similar to a run of toppled dominoes (e.g., Pettijohn, 1957; Yagishita, 1997; Rust, 1984; Potsma and Roep, 1985; Todd, 1996). Imbrications may lead to armor development and the interlocking of clasts. As a consequence the search for possible controls on the formation of this fabric has received major attention in the literature (e.g., Bray and Church, 1980; Carling, 1981; Aberle and Nikora, 2006).

In the past decades, the occurrence of clast imbrications in streams has been considered to record high stage flows (Rust, 1978; Miall, 1978; Sinclair and Jaffey, 2001). The related conditions could possibly correspond to the upper flow regime, where the flow velocity of a stream v exceeds the wave's celerity c (Allen, 1997), i.e. the speed of a wave on the water surface. The ratio v/c between these velocities has been referred to as the Froude number F where in theory $F>1$ denotes upper flow or supercritical conditions, while $F<1$ is characteristic for the lower flow regime or alternatively subcritical conditions (Engelund and Hansen, 1967). A hydraulic jump, which is characterized by a distinct increase in flow surface elevation and a decrease in flow velocity, then marks the downstream transition from a super- to a subcritical flow (Figure 1A). These hydrological conditions are particularly mirrored by the surface texture in relation to water depth. Surface waves that form under subcritical conditions have wavelenghts that are smaller than the water depths (Figure 1B). The surface waves tend to migrate and fade out in the upstream direction with respect to the flow. Contrariwise, the wavelengths of standing waves, which represent one possible characteristic feature of supercritical conditions ($F\approx1$), are significantly larger than the corresponding water depths, and the surface waves are stationary. Hydraulic jumps are manifested themselves by a sudden deceleration of the flow velocity and by an overturning of the flow surface (Figure 1).

Significant sediment accumulation may occur underneath the hydraulic jump upon deceleration of the flow's velocity (Slootman et al., 2018). Contrariwise, a downstream change from a lower to an upper flow regime occurs gradually and has no distinct surface expression, neither in terms of flow depth nor flow surface texture. While these mechanisms have been well explored and frequently reported both from modern environments (e.g., Figure 1) and fine grained stratigraphic records (Alexander et al., 2001; Schlunegger et al., 2017; Slootman et al., 2018) and illustrated on photos from the field (Spreafacio et al., 2001), less evidence for an upper flow regime has been documented from the coarse grained fraction of clastic sediments such as conglomerates. This even led Grant (1997) to note that upper flow regime conditions in fluvial channels are rare, and that the use of the Froude number for constraining flood and palaeo-flood measurements lacks justification from sedimentary records. In the same sense, Jarrett (1984) and Trieste (1992, 1994) considered that reports of inferred supercritical flows might be biased by underestimations of the bed roughness in mountainous streams. Nevertheless, the surface texture of the flow illustrated in Figure 1A is characteristic for many mountainous streams (Spreafico et al., 2001), where hydraulic jumps are observed on the stoss side of large imbricated clasts. In addition, because the entrainment of large clasts such as cobbles and boulders does involve large shear stresses and thus high discharge flows (Rust, 1978; Miall, 1978; Sinclair and Jaffey, 2001), it is possible that the transport and deposition of these particles, and particularly the formation of an imbricated fabric, may occur during supercritical flows. Here, we explore the validity of this hypothesis for modern coarse-grained streams and stratigraphic records, and we calculate the related hydrological conditions. Similar to Grant (1997), we determine the Froude number at conditions of incipient motion of coarse-grained bedload for various bed roughness and stream gradient values. We then compare the results with data from modern streams in the Swiss Alps, stratigraphic records and published results of laboratory experiments.

2 **Methods**

2.1 Expressions relating flow regime to channel gradient and bed roughness

Channel depth and grain size are the simplest and most straightforward variables that can be extracted from stratigraphic records (Duller et al., 2012). It has been shown that quantitative information about these variables can be used as basis to calculate palaeo-slope and roughness values of streams for the geologic past (Paola and Mohring, 1996; Duller et al., 2012; Schlunegger and Norton, 2015; Garefalakis and Schlunegger; 2018). We therefore decided to focus on the simplest expressions relating channel depth and grain size to flow strength and sediment transport, such as that the resulting formulas can also be applied to geological records. We are aware that this will be associated with large generalizations and simplifications, which will not consider the entire range of complexities that are usually associated with the transport of coarse-grained bedload in streams.

2.2 Boundary conditions

In the following, we consider the hydrological situation at the incipient motion of coarse-grained bedload. For these conditions, the dimensionless Shields parameter ϕ can be computed, which is the ratio between the shear stress exerted by the fluid on the bed τ_{cDi} and the particle's inertial force at the incipient motion (Shields, 1936; Paola et al., 1992; Paola and Mohring, 1996; Tucker and Slingerland, 1997):

$$\phi = \frac{\tau_{cDi}}{(\rho_s - \rho) g D_i} \qquad (1a).$$

Here, τ_{cDi} denotes the critical shear stress, or alternatively the Shields stress, which is required to shift a sediment particle with the grain size D_i. The constants ρ_s (2700 kg/m^3) and ρ denote the sediment and water densities, and g is the gravitational acceleration. The relationship expressed in equation (1a) predicts that a sediment particle with diameter D_i will be transported if the ratio between the fluid's shear stress τ_{cDi} and the particle's inertial force equals the value of ϕ. Assignments of values to ϕ vary considerably and largely range between c. 0.03 and 0.06, depending on the site-specific arrangement, the sorting, and the interlocking of the clasts (Buffington and Montgomery, 1997; Church, 1998). This also includes the hiding and protrusion of small and large clasts, respectively, which may exert a strong influence on the threshold conditions upon clast entrainment (e.g., Egiazaroff, 1965; Parker et al., 1982; Andrews, 1984; Kirchner et al., 1990). In the same sense, a smooth and flat channel bed surface, which may be a well-armored channel floor with well-sorted clasts, is likely to offer a greater resistance for the entrainment of a sediment particle than a gravel bar with a poorly sorted arrangement of the bed material (Egiazaroff, 1965; Buffington and Montgomery, 1997).

The relationships denoted in equation (1a) differ for the case of channel forming floods. At these conditions, channel forming Shield stresses $\tau_{channel}$ are up to 1.2 times (Parker, 1978) above the threshold τ_{cDi} for the initiation of motion. Pfeiffer et al. (2017) additionally showed that some rivers have $\tau_{channel}/\tau_{cDi}$. ratios that are even higher. The consideration of channel forming floods thus requires larger thresholds and thus a modification of equation (1a), which then takes the following form:

$$\phi' \geq \frac{\tau_{channel}}{(\rho_s - \rho)gD_i} \approx 1.2\frac{\tau_{cDi}}{(\rho_s - \rho)gD_i} = 1.2\phi \qquad (1b).$$

Equation (1a) can then be transformed to an expression, which quantifies the critical shear stress for the entrainment of a sediment particle with a distinct grain size D_i:

$$\tau_{cDi} = \phi(\rho_s - \rho)gD_i \qquad (2).$$

Among the various grain sizes, the D_{84} grain size has been considered as more suitable for the characterization of the gravel bar structure than the D_{50} (Howard, 1980; Hey and Thorne, 1986; Grant et al., 1990). In addition, the D_{84} has also been considered as a valuable parameter for the quantification of the relative bed roughness, which is defined as the ratio between grain size and water depth (e.g., Wiberg and Smith, 1991). If this inference is valid, then a major alteration of channel-bar arrangements requires a flow strength that is large enough to entrain the grain size represented by the 84th percentile.

Based on the results of flume experiments (Meyer-Peter and Müller, 1948) and observations in the field (Andrews, 1984), a Shields variable of ϕ=0.047 has conventionally been employed in a large number of studies (e.g., Paola and Mohring,

1996) particularly if the D_{50} is considered. Note that a re-analysis (Wong and Parker, 2006) of the Meyer-Peter and Müller equation (1948) returned values of ϕ=0.0495≈0.05, which we thus applied in this paper. However, experiments also showed that material transport can occur at much lower thresholds where ϕ-values are as low as 0.03 (Ferguson, 2012; Powell et al., 2016). A ϕ-value of 0.03 might particularly be an appropriate threshold for the entrainment of the D_{84}, because of possible protrusion effects (e.g., Kirchner et al., 1990). Finally, Mueller et al. (2005) and Lamb et al. (2008) proposed that ϕ depends on channel gradients, where ϕ (for the D_{50} grain size) might exceed 0.1 for channels that are steeper than 1.1°. It appears that the thresholds for the entrainment of sediment strongly vary according to site and experiment specific conditions. We therefore employed the entire range of ϕ-values from 0.03 to 1.1 to comply with these complexities, which also includes channel forming floods (Parker, 1978).

2.3 Hydrology, bed shear stresses and incipient motion of clasts

Bed shear stress is calculated using the approximation for an uniform flow down an inclined plane (e.g. Tucker & Slingerland, 1997), where:

$$\tau = g\rho S d \qquad (3).$$

Here, S denotes the channel gradient, and d is the water depth. This relationship has been considered as adequate for streams with a steady, uniform flow, and where channel widths are more than 20 times larger than water depths, which is commonly the case for most rivers (Tucker and Slingerland, 1997).

Alternatively, bed shear stresses can also be computed as a function of the kinetic energy (Ferguson, 2007), where:

$$\tau = \frac{f}{8}\rho v^2 \qquad (4).$$

In this relationship, v is the flow velocity. The variable f, referred to as the Darcy-Weisbach friction factor (e.g., Papaevangelou et al., 2010), denotes the energy loss due to friction within the roughness layer at the bottom of the flow. It also considers skin friction effects within the flow column (Ferguson, 2007). These relationships illustrate that assignments of values to f are complicated and vary considerably. Ferguson (2007) reduced these complexities to a single expression (equation 5), where he considered roughness-layer (Krogstad and Antonia, 1999) and skin friction effects on the velocity of a water column at its surface. In the Ferguson (2007) relationship, f depends on water depths d relative to the grain size D_{84} and thus on the relative bed roughness:

$$\frac{f}{8} = \frac{\left(\frac{D_{84}}{d}\right)^2}{a_2^2} + \frac{\left(\frac{D_{84}}{d}\right)^{1/3}}{a_1^2} \qquad (5).$$

Here, a_1 and a_2 are constants that vary between 7–8 and 1–4, respectively (Ferguson, 2007). A calibration of equation 5 by Ferguson (2007), where the D_{84} was employed as the threshold grain size, returned values of 7.5 and 2.36 for a_1 and a_2, respectively, which we adapt in this paper. We additionally considered possible consequences of energy loss through assignments of different values to the Shields (1936) variable (see explanation of equation 1a above). We are aware that we could also employ the Manning's number *n* for the characterization of the channel's fabric (Whipple, 2004) and the relative bed roughness (Jarrett, 1984). Related expressions deviated by Jarrett (1984) predict that the Manning's number *n* hinges on the channel gradient and water depth only and does not consider a dependency on the bed structure. We thus prefer to use Ferguson's (2007) approach (eq. 5), which explicitly includes the relative bed roughness, consistent with the most recent work by Wickert and Schildgen (2018, see their equation 13).

As outlined in the introduction, the Froude number F can be approximated through the ratio between the flow velocity v and the celerity of a surface wave c. For shallow water conditions, which is commonly the case for rivers and streams, this relationship can be computed if the water depth d is known:

$$F = \frac{v}{c} = \frac{v}{\sqrt{gd}} \quad (6).$$

Combining equation 3, 4, and 6 yields then a simple expression where:

$$F = \sqrt{8\frac{S}{f}} \quad (7).$$

This expression states that the flow regime, expressed here by the Froude number F, depends on two partly non-related variables. In particular, for a given bed friction f, which depends on the bed roughness (Ferguson, 2007), upper flow regime conditions tend to establish for steep channels. Contrariwise, lower regime flows may occur in a steep environment where poorly sorted material exerts a large resistance on the flow, thereby reducing the flow velocity and hence the Froude number. Accordingly, where the entrainment of sediment particles can be expressed through the Shields (1936) variable ϕ, the dependency of F on the channel gradient S can be computed through the combination of equations 2, 3, 5 and 7:

$$F = \sqrt{\frac{S}{\left(\frac{\rho S}{\phi(\rho_s-\rho)}\right)^2 * a_2^{-2} + \left(\frac{\rho S}{\phi(\rho_s-\rho)}\right)^{1/3} * a_1^{-2}}} \quad (8).$$

Alternatively, also during channel forming floods, an expression where the Froude number depends on the bed roughness D_{84}/d only can be achieved through the combination of equations 2, 3 and 7:

$$F = \sqrt{8 * \frac{\phi(\rho_s - \rho)}{\rho * f} * \frac{D_{84}}{d}} \qquad (9).$$

We thus used equations 8 and 9 to calculate the Froude numbers at the incipient motion of the D_{84} grain sizes. We then compared these results with data from modern streams and stratigraphic records.

2.4 Collection of data from modern streams and stratigraphic records

We used observations about clast arrangements in gravelly streams in Switzerland. We paid special attention to the occurrence of clast imbrications, as we hypothesize that this fabric may document the occurrence of upper flow regimes (Figure 1) upon sedimentation and gravel bar migration. We selected those sites for which Litty and Schlunegger (2017) reported grain size data (Table 1). At these locations, we explored multiple gravel bars for the occurrence or absence of clast imbrications over a reach of several hundreds of meters. We then determined a mean energy gradient over a c. 500 m-long reach, which we calculated from topographic maps at scales 1:10'000.

The selected streams are all situated around the Central Alps (Figure 2), have various upstream drainage basins and different source rock lithologies (Spicher, 1980) and grain size distributions. At sites where grain size data has been collected, the ratio between the clasts' medium *b*- and longest *a*-axes are constant and range between 0.67 and 0.72 irrespective of the grain size distribution in these streams (Litty and Schlunegger, 2017). For these sites, we calculated the bed roughness D_{84}/d at the incipient motion of the D_{84}. Here, related water depths d were determined through the combination of equations (2) and (3), and using the channel gradient S at these sites.

The Swiss Federal Office for the Environment (FOEN) estimated the Froude numbers for various flood magnitudes of selected streams situated on the northern side of the Swiss Alps (Spreafico et al., 2001; see Figure 2 for location of sites). These estimates are based on flow velocities, flow depths and cross-sectional geometries of channels. The authors of this study also determined the corresponding channel gradient over a reach of several hundred meters. Because we will calculate the dependency of the Froude number on the channel gradient and the thresholds for the entrainment of sediment, expressed through different ϕ-values, we will use the Spreafico et al. (2001) dataset to constrain the range of possible ϕ-values for streams in Switzerland.

We finally identified possible relationships between channel gradient, bed roughness, and the occurrence of clast imbrications from stratigraphic records. We focused on the Late Oligocene suite of alluvial megafan conglomerates (Rigi and Thun sections, Figure 2) deposited at the proximal border of the Swiss Molasse basin. For these conglomerates, Garefalakis and Schlunegger (2018) and Schlunegger and Norton (2015) collected data about the depth and gradient of palaeo-channels, and information about the grain size distribution along c. 3000 to 3600 m-thick sections (Table 1). We returned to these sections and examined c. 50 sites for the occurrence of clast imbrications along the conglomerate suites.

3 Results

3.1 Calculation of flow regimes as a function of bed roughness and channel gradient

We calculated the Froude numbers F for different values of channel gradient S, bed roughness D_{84}/d and threshold conditions ϕ for the incipient motion of material, and we compared these results with observations from modern streams and stratigraphic records. We avoided calculation of the Froude numbers for slopes steeper than 1.4° because channels tend to adapt a step-pool geometry in their thalwegs (Whipple, 2014), for which our simple calculations might no longer apply. We set the thresholds for critical flow conditions to a Froude number F=0.9, which is consistent with estimations for the formation of upper flow regime bedforms by Koster (1978). Calculations were initially carried out using a Shields variable of ϕ=0.0495≈0.05, as this value has commonly been used in a large number of studies (see above). The results reveal that the Froude number increases with steeper channels (Figure 3A) and reaches the field of critical conditions for ~0.5° slopes. The values reach a maximum of nearly 1 where channel gradients are between ~0.8°–1°. Froude numbers then slightly decrease for channels steeper than 1° and finally reach a value of 0.9 for gradients >1.2°. In the case of greater thresholds for the incipient motion of clasts, which is expressed through a larger Shields (1936) variable of ϕ =0.06, flows adapt supercritical conditions for channels steeper than ~0.4°. For cases where the thresholds for the entrainment of the material are less (expressed here through a lower Shields (1936) variable of ϕ=0.03), streams remain in the lower flow regime.

The Froude number pattern is quite similar for increasing bed roughness (Figure 3B). For threshold conditions expressed through a Shields (1936) variable ϕ =0.0495≈0.05, the Froude numbers increase with higher relative bed roughness. Supercritical conditions are reached for a bed roughness of c. 0.1, after which the Froude numbers decrease with greater roughness. At larger threshold conditions for sediment entrainment, expressed through a Shields variable ϕ =0.06, upper flow regime conditions might prevail for bed surface roughness values between 0.06 and 0.5. Smaller and larger roughness values will keep the flow in the lower regime. Contrariwise, the stream will not shift to the upper regime for ϕ-values as low as 0.03. Note that the consideration of the full range of roughness-layer and skin friction effects, expressed through the coefficients a_1 and a_2 in equation (8), shifts the pattern of Froude values to lower and higher values. But this will not alter the general finding that upper flow regime conditions at the incipient motion of gravels might be expected for channel gradients S that are steeper than 0.5°±0.1°, and for a bed roughness D_{84}/d greater than ~0.06.

We also calculated the Froude numbers for a Shields variable of $\phi=0.1$, because observations have shown that thresholds for the entrainment of sediment particles may increase with steeper channels (Mueller et al., 2005; Ferguson, 2012). This might be an exaggeration (Lamb et al., 2008), but will give an upper bound for the dependence of the Froude number on the Shields variable. We additionally considered the case where the Shields (1936) variable depends on the channel gradient S through $\phi=2.81*S+0.021$ (Mueller et al., 2005). These relationships have been established using bed load rating curves, which are based on field surveys in mountainous streams in North America and England. We found that the flows shift to critical conditions for channels steeper than between 0.5° and 0.6° (slope dependent ϕ) and for a bed roughness >0.04 ($\phi=0.1$).

In summary, the calculations predict that water flow may shift to upper flow regime conditions for: (i) ϕ-values larger than 0.05; (ii) slopes steeper than ~0.5°±0.1°; and (iii) relative bed roughness values greater than ~0.06±0.01.

3.2 Estimates of ϕ-values from modern streams in the Central Alps

Spreafico et al. (2001) estimated the Froude numbers for various streams situated on the northern side of the Swiss Alps. Related values range between 0.2 and 1.1 and generally increase together with channel gradients (vertical bars on Figure 3A). The surface expressions of the flows particularly of the Birse and Thur streams (labeled as *b* and *t* on Figure 3A) are characterized by multiple hydraulic jumps (Spreafico et al., 2001, p. 71 and p. 77). Therefore, the inferred small Froude numbers (between 0.6 and 0.9) of these streams have to be treated with caution.

The Froude number estimates by Spreafico et al. (2001) disclose a large scatter in the relationship to the channel gradient (Figure 3A, vertical bars). This can partially be explained by site-specific differences in bed roughness, which are related to anthropogenic corrections and constructions (Spreafico et al., 2001). Nevertheless, the comparison between these data and the results of our calculations reveal that the entire range of ϕ-values between 0.03 and 0.1 has to be taken into account for the hydrological conditions in the streams surrounding the Swiss Alps (Figure 3A). This also implies that the selection of a threshold, expressed by the ϕ-value, warrants a careful justification, which we present in the discussion.

3.3 Data about the occurrence or absence of clast imbrications from modern streams

Here, we present evidence for imbrications and non-imbrications from modern rivers, and we relate these observations to channel slope (Figure 4A) and bed roughness (Figure 4B). Data on grain size, stream runoff and channel morphology are available for several rivers in the northern, the central and the southern part of the Swiss mountain belt. These streams are situated both in the core of the Alps and the foreland. The bedrock-geology of their headwaters includes the entire range of lithologies from sedimentary units to schists, gneisses and granites. In the same sense, the streams cover the full range of water sources in their headwaters including glaciers and surface runoff. Except for the Maggia River between the sites Bignasco and Losone (Figure 2), all streams are channelized, and the rivers generally flow in a bed that is laterally confined by artificial riverbanks. These are either made up of concrete walls or outsized boulders. In this context, information about the hydrographs, grain size and the results of the shear stress calculations consider the time after these constructions have been made.

Channel morphologies

The thalweg of the streams meanders between the artificial walls within a 20 to 50 m-wide belt. Flat-topped longitudinal bars that are several tens of meters long and that emerge up to 1.5 m above the thalweg are situated adjacent to the artificial riverbanks on the slip-off slope of these meanders. They evolve into subaquatic transverse bars, or riffles, farther downstream where the thalweg shifts to the opposite channel margin. Channels are deepest and flattest along the outer cutbank side of the meanders and in pools downstream of riffles, respectively. The thalweg then steepens where it crosses the transverse bars and riffles. This is also the location where some streams show evidence for standing waves with wavelengths >5 m (e.g., at Reuss, Figure 5). Standing waves have also been encountered in the Waldemme River at Littau (Figure 6B) when water runoff at that particular site was c. 100 m^3/s and when rumbling sounds suggested that clasts were rolling or sliding. The streams thus display a complex pattern where channel depths, flow velocities and possibly also hydrological regimes alternate over short distances of tens to hundreds of meters. These arrangements of channel-bar pairs and particularly their positions within the channel belt has been stable over the past years as the locations of the gravel bars are still the same as the ones reported by Litty and Schlunegger (2016).

Streams with evidence for clast imbrication

Inspections of gravel bars have shown clear evidence for imbrications in the Glenner, the Landquart, the Verzasca, and the Waldemme rivers (Table 1). In these streams, channel gradients range between 0.6° (Waldemme) and 1.2° (Glenner) (Figure 4A). The sizes of the D_{84} range between 3 cm (Waldemme) and 12 cm (Glenner). The gravel lithology includes the entire variety from sedimentary (Waldemme) to crystalline constituents (Glenner, Landquart, Verzasca). The inferred bed roughness at the incipient motion of the D_{84} includes the range between c. 0.125 (Waldemme) and 0.31 (Glenner) (Figure 4B). In these streams, bars with imbricated clasts alternate with pools over a reach of several hundreds of meters.

At Maggia, Reuss and Waldemme Littau, the largest clasts are arranged as triplets or quadruplets of imbricated constituents within generally flat lying to randomly-oriented finer grained sediment particles. The density of these arrangements ranges between 5 groups per 10 m^2 (Maggia Bignasco, Maggia Losone) to c. 10 groups per 10 m^2 (Maggia Visletto, Reuss, Waldemme Littau e.g. Figure 6D). The channel gradients at these sites span the range between c. 0.3 and 0.6°, and the D_{84} clasts are between 3 and 9 cm large (Reuss and Maggia Visletto). Accordingly, the relative bed roughness at the incipient motion of the D_{84} ranges between 0.07 and 0.16.

At all sites mentioned above, clasts on subaquatic and subaerial gravel bars are generally arranged as well-sorted and densely packed clusters, possibly representing incipient bedforms (e.g., Figure 6D). In most cases, grains imbricate behind an outsized clast, which usually delineates the front of imbricated arrangements of sediment particles. In addition, the lowermost 10-20% part of most of the large clasts is embedded, and thus buried, in a fine-grained matrix, which was most likely deposited during the waning stage of a flood. Isolated, non-buried clasts that are flat lying on their *a*-*b*-planes do occur but are less frequent than embedded clasts or constituents arranged in clusters. The inclination dip of the *a*-*b*-planes ranges between c. 20-40° (Figure 6D). Finally, streams with clast imbrications display surface expressions, which point to an upper flow regime during low (e.g., Reuss, Figure 5B) and high-water stages (e.g., Waldemme, Figure 6B).

Streams with little or no evidence for clast imbrication

Gravel bars within the Emme stream are made up of generally flat lying gravels and cobbles. A small tilt of <10° of *a*-*b*-planes occurs where individual clasts slightly overlap each other, similar to a shingling arrangement of particles. This is particularly the case in pools and on the upstream stoss-side of longitudinal and transverse bars where channel gradients are flat. Also in the Emme River, clast imbrications occur in places only where gravel bars have steep downstream slip faces, which are mainly observed at the end of transverse bars. At sites where imbrication is absent, most of the clasts are lying flat on their *a*-*b*-planes, and embedding by finer-grained material is less frequently observed than in streams with clast imbrications. The channel gradient is less than 0.5°, and the size of the D_{84} measures 2 cm. The bed roughness of this stream, calculated for the incipient of motion of the 84^{th} grain size percentile, ranges between 0.07 and 0.10. Finally, the flow displays a smooth surface expression during low- and high-water stages (Spreafico et al., 2001, p. 53), which is a characteristic evidence for lower flow regime conditions.

The channel morphology of the Sense River differs from that of the Emme stream in the sense that bedrock reaches alternate with alluvial segments over a wavelength of 100-200 meters and more. Alluvial segments are flat (c. 0.3°) and host lateral and transverse gravel bars where the D_{84} measures 6 cm. On top of these bars, gravels are generally lying flat on their *a*-*b*-planes (Figure 6C). Imbrications are observed where some of these gravels are overlapping each other, resulting in a dip angle of 10-20°. Contrariwise, bedrock reaches (site *S'* on Figure 4A) that form distinct steps in the thalweg are up to 0.5° steep and partly covered by subaquatic longitudinal bars (Figure 1B) where imbricated clasts alternate with flat-lying grains at the meter scale. The channel bed surface is generally well-sorted and well-armored where clasts are either interlocked, partly isolated, and also rooted in a finer-grained matrix, as a photo of a subaquatic longitudinal bar shows (Figure 6A). At these sites, upper flow regime segments laterally change to lower flow regime reaches over short distances of a few meters (Figure 1B). While we have made this observation during low water stages only, it is very likely that sub- and supercritical flows also change during flood stages over short distances, as various examples of Alpine streams show (Spreafico et al., 2001).

3.4 Data about the occurrence or absence of clast imbrications from stratigraphic records

Here, we calculated patterns of bed roughness and related channel gradients and explored c. 50 conglomerate sites for the occurrence or absence of clast imbrications. We used published data about channel depth d, surface gradients S and information about the pattern of the D_{84}, which have been reported from the Late Oligocene alluvial megafan conglomerates at Rigi (47°03'N / 8°29'E) and Thun (46°46'N / 7°44'E) situated in the Molasse foreland basin north of the Alpine orogen (Figure 2, Table 1). The depositional evolution of these conglomerates has been related to the rise of the Alpine mountain belt and the associated erosional history of this orogen (Kempf et al., 1999; Schlunegger and Castelltort, 2016).

The deposits at Rigi are c. 3600 m thick and made up of an alternation of conglomerates and mudstones (Stürm, 1973) that were deposited between 30 and 25 Ma according to magneto-polarity chronologies and mammal biostratigraphic data (Engesser and Kälin, 2017). Garefalakis and Schlunegger (2018) subdivided this alternation of conglomerates and mudstones into four segments labeled as α through δ. The lowermost segments α and β are an alternation of mudstones and conglomerate beds and were deposited by gravelly streams (Stürm, 1973). According to Garefalakis and Schlunegger (2018), the depositional area was characterized by a low surface slope ranging between 0.2±0.06° and 0.4±0.2°. Channel depths span the range between 1.7 and 2.5 m, and the D_{84} values are between 2 and 6 cm. These measurements result in bed roughness values between 0.02 and 0.05. Except for one site, we found no imbrications in outcrops of α and β units (Figures 4, 7A).

The top of the Rigi section, referred to as segments γ and δ by Garefalakis and Schlunegger (2018), is an amalgamated stack of conglomerate beds deposited by non-confined braided streams (Stürm, 1973). Garefalakis and Schlunegger (2018) inferred values between 0.65±0.2° and 0.9±0.4° for the palaeo-gradient of these rivers (Table 1). D_{84} values range between 6 and 12 cm, and palaeo-channels were c. 1.2 m deep. This yields a relative bed roughness between c. 0.05 and 0.12. Interestingly, a large number of conglomerate sites within the segments γ and δ display evidence for clast imbrications in outcrops parallel to the palaeo-discharge direction (Figures 4, 6B). In addition, some outcrops show sedimentary structures that correspond to cluster bedforms of imbricated clasts (*C* on Figure 7B). However, at all sites, the lateral extents of groups with imbricated clasts are limited to widths of 1-2 meters. Please refer to Garefalakis and Schlunegger (2018) and their Figure 2 for location of sites displaying units α through δ.

The up to 3000 m-thick conglomerates at Thun are slightly younger, and the ages span the time interval between c. 26 and 24 Ma according to magneto-polarity chronologies (Schlunegger et al., 1996). Similar to the Rigi section, the conglomerates at Thun start with an alternation of conglomerates, mudstones and sandstones, which has been referred to as unit A. This suite is overlain by an up to 2000 m-thick amalgamated stack of conglomerate beds (unit B). Channel depths within unit A range between 3 to 5 m, and streams were between 0.1° and 0.3° steep. Channels in the overlying unit B were shallower and between 1.5 and 3 m deep. Stream gradients varied between 0.4° and 1°, depending on the relationships between inferred water depths and maximum clast sizes (Schlunegger and Norton, 2015). In outcrops parallel to the palaeo-discharge direction, sequences with imbricated clasts have only been found in unit B where palaeo-channel slopes were steeper than 0.4° (Figure 4A). Similar to the Rigi section, the lateral extents of groups with imbricated clasts are limited to widths of a few meters only. No data is available for computing the D_{84} grain size, with the consequence that we cannot estimate the bed roughness for the Thun conglomerates. Please see Schlunegger and Norton (2015) for location of sites where units A and B are exposed.

Similar to the modern examples, imbricated clasts form a well-sorted cluster and commonly include the largest constituents of a gravel bar. In most cases, clasts imbricate behind an outsized constituent, which usually delineates the front of an imbricated arrangement of clasts (Figure 7B).

4 Discussion

4.1 Selection of preferred boundary conditions

Our calculations reveal that the results are strongly dependent on: (i) the selection of values for the Shields variable ϕ; (ii) the way of how we consider variations in slope *S* at the bar and reach scales, and (iii) the consideration of flood magnitudes which either result in the motion of individual sediment particles or the alteration of the shape of an entire channel (channel forming floods). This section is devoted to justify the selection of our preferred boundary conditions.

Thresholds regarding channel forming floods versus incipient motion of individual clasts

We constrained our calculations on the incipient motion of individual clasts and used equation (1a) for all other considerations. This approach might be perceived as a large contrast to the hydrological conditions during channel forming floods where thresholds for the evacuation of sediment are up to 1.2 times larger, as theoretical and field-based analyses and have shown (Parker, 1978; Philips and Jerolmack, 20916; Pfeiffer et al., 2017). Nevertheless, the consequences on the outcome of our calculations are minor, at least when the Froude number dependencies on the slope and bed roughness parameters are considered. In fact, a 1.2-times larger threshold will increase the ϕ–values (equation 1b) to the range between 0.036 and 0.072. However, as illustrated in Figure 3, this will not change the general pattern. In addition, while channel forming floods are mainly associated with equal mobility of a large range of sediment particles, the formation of an imbricated fabric involves the clustering of individual clasts only. We use these arguments to justify our preference for using equation 1a (incipient motion of clasts) rather than equation 1b (channel forming floods).

Protrusion and hiding effects and consequences for the selection of ϕ–values

Larger bed surface grains, as is the case for most of the imbricated clasts, may exert lower mobility thresholds because of a greater protrusion and a smaller intergranular friction angle, as noted by Buffington and Montgomery (1997) in their review. Related consequences have been explored in experiments (e.g., Buffington et al., 1992) and through field-based studies, which were likewise complemented with experiments in the laboratory (Johnston et al., 1998). These studies resulted in the notion that the entrainment of the largest clasts (e.g., the D_{84}) most likely requires lower flow strengths than the shift of median-sized sediment particles. As a consequence, while ϕ-values might be as high as 0.1 for the displacement of the D_{50} (Buffington et al., 1992), conditions for the incipient dislocation of large clasts could be significantly different. In particular, for clasts that are up to five times larger than the D_{50} (which corresponds to the ratio between the D_{84} and the D_{50} of the Swiss data, Table 1), Buffington et al (1992) and also Johnston et al. (1998) predicted ϕ–values that might be as low as 0.03 or even less. Related ϕ–values, for instance, have indeed been applied for mountainous streams where the supply of sediment from the lateral hillslopes has been large (van der Berg and Schlunegger, 2012). Large sediment fluxes have been considered to result in a poor sorting and a low packing of the material, and thus in low thresholds particularly for the incipient motion of large clast (Lenzi et al., 2006; van der Berg and Schlunegger, 2012). Our calculations predict that an upper flow regime is very unlikely to establish at these conditions (ϕ–value of 0.03).

However, we consider it unlikely that the formation of most of the imbrications, as we did encounter in the analyzed Alpine streams and in the stratigraphic record, were associated with thresholds as low as those proposed by e.g., Lenzi et al. (2006) and van der Berg and

Schlunegger (2012). We base our inference on the observation that the analyzed gravel bars display an arrangement where large clasts are generally well sorted and densely packed, both on subaerial (during low water stages) and subaquatic bars. This results in a high interlocking degree of sediment particles within the bars we have encountered in the field. In addition, field inspections showed that the base of most of the large clasts, particularly those in subaquatic bars, are embedded and thus buried in finer grained material, and only very few clasts are lying isolated and flat on their *a-b*-planes. This implies that the fine-grained sediment particles have to be removed before these clasts can be entrained. In this case, hiding effects associated with ϕ-values >0.5 would possibly be appropriate for the prediction of material entrainment of the finer-grained sediments before the larger clasts can be shifted (Buffington and Montgomery, 1997). As a consequence, a dislocation of these clasts and thus a rearrangement of the sedimentary fabric most likely require that large thresholds have to be exceeded, which is mainly accomplished through high-discharge events with large flow strengths. We thus propose that the use of ϕ–values of c. 0.05, which is commonly used for the entrainment of the D_{50} (Paola and Mohring, 1996), is also adequate for the calculation of the hydrological conditions associated with the fabric we have encountered in the field. We do acknowledge, however, that this hypothesis warrants a test with quantitative data, which we have not available. Please note that the low Froude numbers and thus the low ϕ-values of 0.3 inferred for the Thur and the Birse streams might be underestimated, because photos that were taken during high stage flows of these streams display clear evidence for multiple hydraulic jumps over m-long reaches (Spreafico et al., 2001, p. 71 and 77).

Variations in channel gradient at the bar and reach scales

Figure 3 shows that the results largely hinge on the values of ϕ and *S*. We applied equation 3 while inferring a steady uniform flow and a bed slope, which is constant over a distance of 500 m. We did not consider any smaller-scale slope variations that are caused by downstream alternations of bars, riffles and pools as we lack the required quantitative information. This inference results in an energy slope, which is neither equal to the water surface slope nor to the bed slope. Such inequalities increase substantially when unsteady non-uniform super-critical flows and transitions are considered (e.g., Figure 1A), which is not fully described by equations 3 and 4, and which introduces a bias. These variations in channel floor morphologies are likewise not depicted in experiments either (e.g., Buffington et al., 1992; Powell et al., 2016), which could partially explain the low ϕ-values that result from these studies. We justify our simplification because we are mainly interested in exploring whether supercritical flows are likely to occur for particular ϕ– and channel gradient values.

4.2 Relationships between channel gradient, bed roughness and flow regime

We have found an expression where the Froude number *F*, and thus the change from the lower to the upper flow regime, depends on the channel gradient *S* and the bed roughness D_{84}/d (eq. 7). This relationship also predicts that the controls of both parameters on the Froude number are to some extent independent from each other. Under these considerations, the similar pattern of how the Froude number *F* depends on channel gradient and bed roughness (Figure 3) appears unexpected. However, we note that we computed both relationships for the case of the incipient motion of the grain size percentile D_{84}. This threshold is explicitly considered by equation 2, which we used as basis to derive an expression where the Froude number depends on the channel gradient or the bed roughness only. Therefore, it is not surprising that the dependencies of the Froude number on gradient and bed roughness follow the same trends. In addition, Blissenbach (1952), Paola and Mohring (1996) and also Church (2006) showed that channel gradient, water depth and grain size are closely related parameters during the entrainment of sediment particles. In particular, channels with coarser grained gravel bars tend to be steeper and shallower than those where the bed material is finer grained (Church, 2006). In the same sense, also in steeper streams, bed roughness values tend to be larger than in flatter channels (Whipple, 2004). We use the causal relationships between these variables to explain the similarity in the patterns illustrated in Figures 3A and 3B.

The tendency towards lower Froude numbers for a channel gradient >1° (ϕ >0.05) and a bed roughness >0.3 (ϕ >0.05) is somewhat unexpected. We explain these trends through the non-linear relationships between slope, water depth, the energy loss within the roughness-layer, and the velocity at the flow's surface.

4.3 The formation of imbrications in experiments

Interpretations of the possible linkages between hydrological conditions upon material transport and the formation of imbrications are hampered because experiments have not been designed to explicitly explore these relationships. In addition, as noted by Carling et al. (1992), natural systems differ from the conditions in experiments because of the contrasts in scales. Nevertheless, it was possible to reproduce the formation of clast imbrications in subcritical flumes (Carling et al., 1992), or at least in the absence of any change in flow regime in many experiments. For instance, Qin et al. (2013) quantified the imbrications that resulted from the experiments by Aberle and Nikora (2006) where flows have been stationary. Carling et al. (1992) additionally showed that the shape of a clast has a strong control on the thresholds for incipient motion, the style of motion, and the degree of imbrication. A similar arrangement of clasts was formed in the experiments by Powell et al. (2016) and Bertin and Friedrich (2018), who reproduced imbrications with low Froude numbers between c. 0.55 and 0.9. Please note that we inferred these numbers from the experimental setup of these authors. Powell et al. (2016) additionally showed that the material can be entrained with ϕ-values as low as 0.03, which is consistent with calculations of Froude numbers for some of the streams in Switzerland. Also during experiments, Johansson (1963) reported particle vibration before entrainment either through rolling or sliding. He noted that imbrication was formed at conditions, which corresponded to the lower flow regime during the flume experiments. Based on field observations, Sengupta (1966) reported examples where imbrication was most likely initiated by the development of current crescents around pebbles that were embedded in sand, and that these processes possibly occurred during lower regime flows. Such eddies preferentially develop at the upstream end of pebbles, which then leads to the winnowing of the fine grained sand at the upstream edge and the tilting of this particular clast. Additional sliding, pivoting and vibrating of these sediment particles might then result in the final imbrication. If this process occurs multiple times and affects the sand-gravel interface at various sites, then an armored bed with imbricated clasts can establish without the necessity of supercritical flows, or changes in flow regimes, as experimental results have shown (Aberle and Nikora, 2006; Haynes and Pender, 2007). Such a fabric may even form in response to prolonged periods of sub-threshold flows, as summarized by Ockelford and Haynes (2013). Finally, using flume experiments in a 0.3 m-wide, 4 m-long, recirculating tilting channel flume, Brayshaw (1984) was able to reproduce cluster bedforms with imbricated clasts during subcritical flows (F-numbers between 0.03 and 0.07).

However, inspections of photos illustrating the experimental set up reveal that the surface grains are either flat lying on finer-grained sediments before their entrainment (Figure 3 in Powell et al., 2016), occur isolated on the ground (Figure 2.1b in Carling et al., 1992), or have a low degree of interlocking (Figure 3a in Lamb et al., 2017). Interestingly, the experiment by Buffington et al. (1992) followed a different strategy, where a natural bed-surface of a stream was peeled off with epoxy. They subsequently used this peel in the laboratory to approximate a natural channel bed surface (see their Figure 4), on top of which they randomly placed grains with a known size distribution. Buffington and co-authors then measured the friction angle of the overlying grains, based on which they calculated the critical boundary shear stress values ϕ. In all experiments, the surface morphology of the sedimentary material is flat and lacks topographic variations, which we found as reach-scale alternations of riffles, transverse bars and pools in the field. The low ϕ–values of 0.03, which appears to be typical of bed surface conditions that develop in laboratory flumes (Ferguson, 2012), as summarized by Powell et al. (2016), could possibly be explained by these conditions. Furthermore, and probably more relevant, the lengths of the experimental reaches are generally less and range between e.g., 4.0 meters (Brayshaw, 1984), 4.4 meters (Powell et al., 2016), 15 meters (e.g., Lamb et al., 2017) and even 20 meters (Aberle and Nikora, 2006). We acknowledge that in most experiments the variables have been normalized through an e.g., constant Reynolds or Froude number

(Brayshaw, 1984). This normalization also includes the experimental D_{50}-grain sizes, which are very similar to those we have determined for our selected streams (Litty and Schlunegger, 2017). Nevertheless, we find it really hard to upscale some of the results associated with these experiments to our natural cases where standing waves of 1 m, and even between 5 and 8 meters lengths may occur (our Figures 1B, 5B, 6B), which are not reproducible in the experiments. In addition, Powell et al. (2016) observed that the water surface stayed relatively stable during their experiments, and that the flows were steady and uniform without hydraulic jumps. This contrasts to our natural cases where upper and lower flow regimes alternate over short distances even during low-stage flows. Finally, while winnowing of fine grained material, tilting of clasts and subsequent bed armouring might be a valuable mechanism for the explanation of imbrications during low stage flows in experiments, we consider it unlikely that these results can be directly translated to our field observations. We base our inference on two closely related arguments. First, our reported groups of imbricated clasts tend to be arranged as cluster bedforms (e.g., Figures 6D, 7B), which rather form in response to selective deposition of large clasts (Brayshaw, 1984) than selective entrainment of fine-grained material (Figure 6A). Second, observations (Berther, 2012) and calculations (Litty and Schlunegger, 2017) have shown that effective sediment transport in these streams is likely to occur on decadal time scales (and most likely much shorter; van der Berg and Schlunegger, 2012), at least for subaquatic bars. Sediment transport is then likely to occur over a limited reach only. This means that a large fraction of the shifted material per flood has a local source situated in the same river some hundreds of meters farther upstream where bars are also well armored. This possibly calls for large thresholds for the removal of clasts. In addition, on subaerial bars, waning stages of floods result in the deposition of fine-grained material and not in the winnowing of sand, as our observations have shown. Accordingly, while low ϕ–values and thus a lower flow regime might be appropriate for predicting the entrainment of the sediment particles in experiments, greater thresholds and thus larger ϕ–values are likely to be appropriate for our natural examples for the reasons we have explained in above.

4.4 Possible relationships between flow regimes and clast imbrications based on field observations

Here, we provide evidence for proposing that clast imbrications can be linked with supercritical flows provided that the gravel bars form a well-sorted arrangement of densely packed particles with a clast-supported fabric, as we have encountered in our streams. We sustain our inferences with (i) published examples from natural environments; (ii) our observations from Swiss streams; and (iii) the results of our calculations,

For the North Saskatchewan River in Canada, Shaw and Kellerhals (1977) reported gravel mounds on a lateral gravel bar, which have a regular spacing between 2 and 3 meters and a relatively flat top. Shaw and Kellerhals considered these bedforms as antidunes, which might have formed in the upper flow regime. Also in modern gravelly streams, transverse ribs, which are a series of narrow, current-normally orientated accumulations of large clasts, were considered as evidence for the deposition either under upper flow regime conditions, or in response to upstream-migrating hydraulic jumps (e.g., Koster, 1978; Rust and Gostin, 1981). Koster (1978) additionally reported that these bedforms are associated with clast imbrications (Figure 2 in Koster, 1978). Alexander and Fielding (1997) found modern gravel antidunes with well-developed clast imbrications in the Burdekin River, Australia. Finally, Taki and Parker (2005) reported cyclic steps of channel floor bedforms with wave-lengths that are 100–500 times larger than the flow thickness. These bedforms most likely represent chute-and-pool configurations (Taki and Parker, 2005), which could have formed in response to alternations of upper and lower flow regime conditions, as outlined by Grant (1997). In such a situation, the upstream flow on the stoss-side of the bedform may experience a reduction of the flow velocity, with the effect that the flow may shift to subcritical conditions. This could be associated with a hydraulic jump and a drastic reduction of the flow velocity and thus with a drop of shear stresses (Figure 1A). In gravelly streams, such a situation could result in the deposition of clasts. In such a scenario, the site where sediment accumulates most likely migrates upstream (Figure 8).

Inspections of modern gravel bars in the Central European Alps and of stratigraphic records (Figure 4) reveal the occurrence of imbrications where channel slopes are steeper than 0.4°-0.5°, and where the values of bed roughness exceed c. 0.06. The results of our generic calculations (Figure 3) reveal that under these circumstances, flows might become supercritical provided that ϕ–values are greater than c. 0.05 (Figure 3). This is supported by observations form the Waldemme and Reuss Rivers (slope >0.5°) during high stage and low stage flows (Figures 5B and 6B) that provide evidence for standing waves and thus supercritical flows. Contrariwise, the reach of the Emme River is flatter (slope <0.4°), imbrications are largely absent, and flows generally occur in the lower flow regime (Sprefacio et al., 2001, p. 53). We thus propose that a channel gradient of c. 0.5° is critical for both the formation of clast imbrications and possibly also for the establishment of supercritical flows. Based on these relationships, we also suggest that the generation of imbrications may be associated with upper flow regime conditions.

The proposed threshold slope is consistent with the results of previous work, where upper flow regime bedforms such as transvers ribs have been described for e.g., the Peyto Outwash (slope c. 1.09°), the Spring Creek (same slope; McDonald and Banerjee, 1971), and the North Saskatchewan River (slope 0.52°; Dept. Mines and Tech. Survs., 1957). This is also in agreement with observations (Mueller et al., 2005) and the results of theoretical work calibrated with data (Lamb et al., 2008). In particular, Mueller et al. (2005) suggested that a ϕ–value of c. 0.03 is suitable for slopes <0.35°, while ϕ > 0.1 might be more appropriate for the mobilization of coarse-grained sediment particles in channels steeper than 1.1°. This might be an overestimate of the ϕ–dependency of slope (Lamb et al., 2008), but it does show that ϕ–values larger than the commonly used ϕ-values between 0.04 and 0.05 might be appropriate where channels are steep (see also Ferguson, 2012). Finally, Simons and Richardson (1960, p. 45) noted that flows rarely exceeded unity Froude numbers over an extended period of time in a stream with erodible banks. We thus use the conclusion of their discussion to explain the limited spatial extent of individual ensembles of imbricated clasts in modern streams and stratigraphic records.

5 Summary and conclusions

We started with the hypothesis that the transport and deposition of coarse-grained particles, and particularly the formation of an imbricated fabric, may be related to changes in flow regimes. We then calculated the Froude number F at conditions of incipient motion of coarse-grained bedload for various bed roughness and stream gradient values, and we compared the results with data from modern streams and stratigraphic records. The results suggest that imbricated clasts are likely to provide evidence for the occurrence of supercritical conditions particularly at sites where channel gradients are steeper than ~0.5° and where ϕ–values are greater than c. 0.05. We do acknowledge that our field-based inferences are associated with large uncertainties regarding channel gradients and grain size (Litty and Schlunegger, 2017), and that they lack a quantitative measure of the spatial distribution of clast imbrications and clast arrangements (Bertin and Friedrich, 2018). In the same sense, the hydrologic calculations and force balancing approaches are based on the simplest published expressions where water flow is related to sediment transport. Larger complexities, which complicate any considerations of material transport (Engelund and Hansen, 1967), have not been considered. This includes, for instance, large supply rates of sediment (van der Berg and Schlunegger, 2012; Bekaddour et al., 2013), changes in bed morphology, spatial variations in turbulences, the shape and the sorting of grains, the 3D arrangement of clasts (Lamb et al., 2008; Hodge et al., 2009), and more complex hydrological conditions including upper-stage plain beds, hydraulic drops, and standing waves (Johannson, 1963). In addition, the occurrence or absence of imbrications also strongly depends on the shape of the involved clasts (Carling et al., 1992). In particular, clasts with a relatively large c-axis tend to form steeper imbrications compared to those constituents where the c-axis is short. In addition, experimental results of Hattingh and Illenberger (1995) showed that spheres and rods have a higher mobility than blades and discs, which is explained by differences in the related lift and drag forces exerted on each shape-type together with the angle of repose and pivotability of these shape types. Unfortunately, we lack the quantitative dataset to properly address these points. We also acknowledge that imbrications do form during subcritical flows in flume experiments at conditions, which can be characterized by low ϕ–values (Brayshaw, 1984; Carling et al., 1992; Powell et al., 2016; Lamb et al., 2017). However, as already noted above, we find it quite hard to upscale the experimental results (<20 meters) to the reach scale of our observations where standing waves with wavelengths as long as 8 meters have been observed (Figure 6B).

Despite our simplifications, we find evidence for proposing that clast imbrications are likely to be associated with supercritical flows provided that (i) channel gradients are steeper than c. 0.5°±0.1°, and (ii) large clasts are tightly packed, closely arranged as cluster bedforms and partly embedded in finer-grained sediment. Mobilization and rearrangements of these structures require larger thresholds (Brayshaw, 1985), which might be large enough (ϕ–values possibly >0.05) to allow supercritical conditions to occur. These findings might be useful for the quantification of hydrological conditions in coarse-grained stratigraphic archives such as conglomerates. As a further implication, the occurrence of imbrications in clastic sediments may be used to infer a minimum value of 0.5°±0.1° for the palaeo-topographic slope. Such a constraint might be beneficial for palaeo-geographic reconstructions and for the analysis of a basin's subsidence history through the back-stripping of strata (e.g., Schlunegger et al., 1997). Finally, for modern streams, the presence of imbrications on gravel bars with closely packed clasts might be more conclusive for inferring an upper flow regime upon material transport than other bedforms such as transverse ribs or antidunes (Koster, 1978; Rust and Gostin, 1981), mainly because clast imbrications have a better preservation potential and are easier to recognize in the field.

Figure captions

Figure 1: A) Photo showing hydraulic jump, and conceptualization of situation displayed in photo of Figure 1A. *F*=Froude number; *v*=flow velocity, *d*=water depth. B) Photo from Sense River, and cross-sections through reaches with upper and lower flow regimes. Surface waves ($\lambda \approx$ 20-30 cm) tend to fade out towards the upstream direction relative to the flow movement where subcritical flows prevail (section to the left). A hydraulic jump separates segments with a supercritical flow from reaches with a subcritical flow where the bedrock builds a ramp. The reach illustrated by the section to the right is characterized by standing waves with wavelengths $\lambda \approx$ 100 cm. The dashed line illustrates the trace of the plane that separates lower from upper regime flows. Please see Figure 2 for location of photo.

Figure 2: Sites where modern gravel bars in streams were inspected for the occurrence of clast imbrications (blue dots). The figure also shows the locations of the stratigraphic sections where conglomerates were analyzed for their

sedimentary structures. *S*=Sense; *E*=Emme; WE_{I-IV}=Waldemme, *WL*=Waldemme at Littau, *R*=Reuss; *L*=Landquart; *G*=Glenner; M_B, M_V, M_L=Maggia at Bignasco, Visletto and Losone; V_F, V_M, V_L=Verzasca at Frasco, Motta and Lavertezzo. See Table 1 for coordinates of sites.

The black squares are sites where Spreafico et al. (2001) have estimated channel gradients and Froude numbers for low and high-stage flows. *b*=Birse-Moutier, *e*=Emme-Burgdorf, *gl*=Glatt-Fällanden, *g*=Gürbe-Belp, *m*=Minster-Euthal, *l*=Lütschine-Gsteig, *s*=Suze-Sonceboz, *t*=Thur-Stein

Figure 3: Relationships between A) channel slope and Froude number *F*, and B) relative bed roughness and *F*. These were calculated as a function of various Shields (1936) variables ϕ. The pale green field indicates the conditions where an upper flow regime could prevail, while the yellow field delineates the occurrence of lower flow regime conditions. In this context, we set the threshold to a Froude number of c. 0.9. This is consistent with the estimation of parameters for the formation of upper flow regime bedforms by Koster (1978). Note that the bed roughness is the ratio between the D_{84} and the water depth *d* at the incipient motion of that particular size class. The vertical bars on Figure 3A also illustrate the Froude numbers that have been estimated by Spreafico et al. (2001) for the following streams and locations: *b*=Birse-Moutier, *e*=Emme-Burgdorf, *gl*=Glatt-Fällanden, *g*=Gürbe-Belp, *m*=Minster-Euthal, *l*=Lütschine-Gsteig, *s*=Suze-Sonceboz, *t*=Thur-Stein. Please note that the low values for the Thur and Birse Rivers might represent underestimates as these streams show evidence for multiple hydraulic jumps during high stage flows.

Figure 4: This figure relates the occurrence of imbrications (blue bars) or no imbrications (red bars) to A) channel slopes and B) relative bed roughness. Red bars with blue hatches indicate that imbrications have been found in places. Blue bars with red hatches suggest that imbrications dominate the bar morphology, but that reaches without imbrications are also present on the same gravel bar. Data from modern streams are displayed above the horizontal axes, while information from stratigraphic sections are placed below the slope and roughness axes, respectively. *S*=Sense, *S*'=Sense with bedrock reach, *E*=Emme, WE_{I-IV}=Waldemme, *WL*=Waldemme at Littau, *R*=Reuss; *L*=Landquart; *G*=Glenner; M_B, M_V, M_L=Maggia at Bignasco, Visletto and Losone; V_F, V_M, V_L=Verzasca at Frasco, Motta and Lavertezzo. See Table 1 for coordinates of sites, and Figure 2 for locations where data were collected.

Figure 5 A) Reuss River with evidence for standing waves along the thalweg. Othophoto reproduced by permission of swisstopo (BA 18065). Please see Figure 2 for location. B) Transverse and lateral bars in the Reuss River with imbricated clasts on the lateral bar forming a riffle, and standing waves where the thalweg crosses the riffle. The wavelength of the standing wave is c. 5 m. Arrow indicates flow direction. Please see Figures 2 and 5A for location of photo.

Figure 6: Photos from the field. A) Photo of subaquatic longitudinal bar taken along the steep bedrock/gravel bar reach of the Sense River (see Figure 1B for location of photo). The clasts in the foreground are clustered and imbricated, forming the nucleus of a possible cluster bedform. This fabric most likely formed when rolling clasts came to a halt behind the boulder at the front. The clasts in the background are either flat lying or slightly imbricated. Except for a few sites, nearly all grains are either partially buried by finer grained material or interlocked by neighboring clasts. The overlying flow shows evidence for supercritical conditions with standing waves. B) Standing waves with a wavelength of c. 8 m in the Waldemme at Littau. Water fluxes are c. 100 m^3/s. Arrow indicates flow direction. C) Flat lying clasts on a lateral bar in the Sense River. Arrow indicates clasts that are overlapping each other, resulting in a shallow dip of <10° of the overriding clast. D) Imbricated clasts within the Maggia River at Visletto. Arrow indicates flow direction. Please note that the imbricated arrangements of clasts mainly include the largest constituents of the gravel bar in the middle of the photo, and clasts of similar sizes. Therefore, for this set of imbricated clasts, we do not consider that protrusion effects might play a major role. See Figure 2 for location and Table 1 for coordinates.

Figure 7: A) Conglomerates at Rigi with no evidence for clast imbrications. White lines indicate the orientation of the bedding. B) Conglomerates at Rigi with imbricated gravels to cobbles that are arranged as cluster bedforms (*C*). Arrow indicates palaeoflow direction. White line refers to the bedding. Note that the steep dip (>25°) of the *a*-*b*-planes of the imbricated clasts. See Figure 2 for location and Table 1 for coordinates.

Figure 8: Conceptual sketch illustrating the formation of an ensemble of imbricated clasts as time proceeds (A through C). According to this model, the site of sediment accumulation will migrate upstream. F=Froude number; v=flow velocity, d=water depth.

Table 1: Grain size and observational data and that have been collected in the field. See text for further explanations.

Author contribution

FS designed the study and carried out the calculations, PG and FS collected the data, FS wrote the text with contributions by PG, both authors contributed to the analyses and discussion of the results.

Data availability

The authors declare they have no conflict of interest.

Acknowledgements

This research has been supported grant No 154198 awarded to Schlunegger by the Swiss National Science Foundation.

References

Aberle, J., and Nikora, V., Statistical properties of armored gravel bed surfaces, Water Resour. Res., 42, W11414, 2006.

Allen, P.A., Earth Surface Processes, John Wiley and Sons, Oxford, 416 pp., 1997.

Andrews, E.D., Bed-material entrainment and hydraulic geometry of gravel-bed rivers in Colorado, GSA Bull., 95, 371-378, 1984.

Alexander, J., Bridge, J.S., Cheel, R.J., and Leclair, S.F., Bedforms and associated sedimentary structures formed under supercritical water flows over aggrading sand beds, Sedimentology, 48, 133-152, 2001.

Alexander, J., and Fielding, C., Gravel antidunes in the tropical Burdekin River, Queensland, Australia, Sedimentology, 44, 327-337, 1997.

Berther, R., Geomorphometrische Untersuchungen entlang der Entle, Ms. Thesis, Univ. Bern, Bern, Switzerland, 94 p., 2012.

Blissenbach, L., Relation of surface angle distribution to particle size distribution on alluvial fans, J. Sediment. Petrol., 22, 25–28, 1952.

Bekaddour, T., Schlunegger, F., Attal, M., and Norton, P.K., Lateral sediment sources and knickzones as controls on spatio-temporal variations of sediment transport in an Alpine river, Sedimentology, 60, 342-357, 2013.

Bray, D.I., and Church, M., Armored versus paved gravel beds. J. Hydraul. Div., 106, 1937-1940, 1980.

Buffington, J., Dietrich, W.E., and Kirchner, J.W., Friction angle measurements on a naturally formed gravel streambed: Implications for critical boundary shear stress, Water Res. Res., 28, 411-425, 1992.

Buffington, J.M., and Montgomery, D. R., A systematic analysis of eight decades of incipient motion studies, with special reference to gravel-bedded rivers, Water Resour. Res., 33, 1993-2029, 1997.

Bertin, S., and Friedrich, H., Effect of surface texture and structure on the development of stable fluvial armors, Geomorphology, 306, 64-79, 2018.

Brayshaw, A.C., Characteristics and origin of cluster bedforms in coarse-grained alluvial channels, in: Sedimentology of Gravels and Conglomerates, edited by Koster, E.H., and Steel, R.J., Mem. Can. Soc. Petrol. Geol., 10, 77-85, 1984., 1978.

Brayshaw, A.C., Bed microtopography and entrainment thresholds in gravel-bed rivers, GSA Bull., 96, 218-223, 1985.

D'Arcy, M., Roda-Boluda, D.C., and Whittaker, A.C., Glacial-interglacial climate changes recorded by debris flow fan deposits, Owens Valley, California, Quat. Sci. Rev., 169, 288-311, 2017.

Carling, P.A., Armored versus paved gravel beds – discussion. J. Hydraul. Div., 107, 1117-1118, 1981.

Carling, P.A., Kelsey, A., and Glaister, M.S., Effect of bed roughness, particle shape and orientation on initial motion criteria, in: Dynamics of gravel-bed rivers, edited by: Billi, P., Hey, R.D., Throne, C.R., and Tacconi, P., 23-39. John Wiley and Sons, Ltd., Chichester, 1992.

Church, M., Palaeohydrological reconstructions from a Holocene valley fill, Fluvial sedimentology, edited by: Miall, A.D., Mem. Can. Soc. Petrol. Geol., 5, 743-772, 1978.

Church, M., Bed material transport and the morphology of alluvial river channels, Ann. Rev. Earth Planet. Sci., 34, 325–354, 2006.

Department of Miines and Technology Surveys, Atlas of Canada, Geogr. Branch, Ottawa, 1957.

Duller, R.A., Whittaker, A.C., Swinehart, J.B., Armitage, J.J., Sinclair, H.D., Bair, A., and Allen, P.A., Abrupt landscape change post-6Ma on the central Great Plains, USA, Geology, 40, 871-874, 2012.

Engesser, B., and Kälin, D., *Eomys helveticus* n. sp. and *Eomys schluneggeri* n. sp., two new small eomyids of the Chattian (MP 25/MP 26) subalpine Lower Freshwater Molasse of Switzerland, Fossil Imprint, 73, 213–224, 2017.

Engelund, F., and Hansen, E., A monograph on sediment transport in alluvial streams, Teknisk Forlag – Copenhagen, 62 pp., 1967.

Ferguson, R., Flow resistance equations for gravel- and boulder- bed streams. Water Resour. Res., 43, W05427, 2007.

Ferguson, R., River channel slope, flow resistance, and gravel entrainment thresholds, Water Resour. Res., 48, W05517, doi:10.1029/2011WR010850, 2012.

Garefalakis, P., and Schlunegger, F., Link between concentrations of sediment flux and deep crustal processes beneath the European Alps, Sci. Rep., 8, 183, doi:10.1038/s41598-017-17182-8

Grant, G.E., Swanson, F.J., and Wolman, M.G., Pattern and origin of stepped-bed morphology in high gradient streams, western Cascades, Oregon, GSA Bull., 102, 340–352, 1990.

Grant, G.E., Critical flow constrains flow hydraulics in mobile-bed streams: A new hypothesis, Water Resour. Res, 33, 349-358, 1997.

Haynes, H., and Pender, G., Stress history effects on graded bed stability, J. Hydraul. Eng., 33, 343-349, 2007.

Hattingh, J., and Illenberger, W.K., Shape sorting of flood-transported synthetic clasts in a gravel bed river, Sed. Geol., 96, 181-190, 1995.

Hey, R.D., and Thorne, C.R., Stable channels with mobile gravel beds, J. Hydr. Eng., 112, 671-689, 1986.

Hodge, R., Brasington, J., and Richards, K., In situ characterization of grain-scale fluvial morphology using Terrestrial Laser Scanning, Earth Surf. Process. Landf., 34, 954-968, 2009.

Howard, A.D., in: Thresholds in Geomorphology, edited by: Coates, D.R., and Vitek, J.D., Allen and Unwin, Boston, MA, 227-258, 1980.

Jarrett, R.D., Hydraulics of high-gradient streams. J. Hydr. Eng., 110, 1519-1939, 1984.

Johansson, C.E., Orientation of pebbles in running water: a laboratory study, Geogr. Ann., 45, 85-112, 1963.

Johnston, C.E., Andrews, E.D., and Pitlick, J., In situ determination of particle friction angles of fluvial gravels, Water Resour. Res., 34, 2017-2030, 1998.

Kempf, O., Matter, A., Burbank, D.W., and Mange, M., Depositional and structural evolution of a foreland basin margin in a magnetostratigraphic framework; the eastern Swiss Molasse Basin, Int. J. Earth Sci., 88, 253–275, 1999.

Kirchner, J.W., Dietrich, W.E., Iseya, F., and Ikeda, H., The variability of critical shear stress, friction angle, and grain protrusion in water-worked sediments, Sedimentology, 37, 647-672, 1990.

Koster, E.H., Transverse ribs: their characteristics, origin and paleohydrauic significance, in: Fluvial sedimentology, edited by: Miall, A.D., Mem. Can. Soc. Petrol. Geol., 5, 161-186, 1978.

Krogstad, P.A., and Antonia, R.A., Surface roughness effects in turbulent boundary layers, Exp. Fluids, 27, 450-460, 1999.

Lamb, M.P., Dietrich, W.E., and Venditti, J.G., Is the critical Shields stress for incipient sediment motion dependent on channel bed slope?, J. Geophys. Res., 113, F02008, 2008.

Lamb, M.P., Brun, F., and Fuller, B.M., Hydrodynamics of steep streams with planar coarse-grained beds: Turbulence, flow resistance, and implications for sediment transport, Water Resour. Res., 53, 2240-2263, 2017.

Lenzi, M.A., Mao, I., and Comiti, F., When does bedload transport begin in steep boulder-bed streams?, Hydrol. Proc., 20, 3517–3533, 2006.

Li, Z., and Komar, P.D., Laboratory measurements of pivoting angles for applications to selective entrainment of gravel in a current, Sedimentology, 33, 413-423, 1986.

Litty, C., and Schlunegger, F., Controls on pebbles' size and shapes in streams oft he Swiss Alps, J. Geol., 123, 405-427, 2017.

Matter, A.: Sedimentologische Untersuchungen im östlichen Napfgebiet (Entlebuch – Tal der Grossen Fontanne, Kt. Luzern), Eclogae Geol. Helv., 57, 315-428, 1964.

McDonald, B.C., and Banerjee, I., Sediments and bedforms on a braided outwash plain, Can. J. Earth Sci., 8, 1282-1301, 1971.

Meyer-Peter, E., and Müller, R., Formulas for bedload transport, Proceedings of the 2nd meeting of the Int. Assoc. Hydraul. Struct. Res., Stockholm, Sweden. Appendix 2, 39–64, 1948.

Miall, A.D., Fluvial sedimentology: An historical overview, in: Fluvial sedimentology, edited by: Miall, A.D., Mem. Can. Soc. Petrol. Geol., 5, 1-48, 1978.

Middleton, L.T., and Trujillo, A.P., Sedimentology and depositional setting of the upper Proterozoic Scanlan Conglomerate, central Arizone. In: Sedimentology of gravels and conglomerates, edited by: Koster, E.H., and Steel, R.J., Mem. Can. Soc. Petrol. Geol., 10, 189-202, 1984.

Mueller, E.R., Pitlick, J., and Nelson, J.M., Variation in the reference Shields stress for bed load transport in gravel-bed streams and rivers, Water Resour. Res., 41, W04006, 2005.

Ockleford, A.-M., and Haynes, H., The impact of stress history on bed structure, Earth Surf. Process. Landf., 38, 717-727, 2013.

Papaevangelou, G., Evangelides, C., and Tsimopoulos, C., A new explicit relation for friction coefficient f in the Darcy-Weisbach equation, Proc. 10th Conf. Prot. Restor. Env., PRE10, July 6-9, 2010.

Paola, C., Heller, P.L., and Angevine, C., The large-scale dynamics of grain-size variation in alluvial basins, 1: Theory, Basin Res., 4, 73-90, 1992.

Paola, C, and Mohring, D., Palaeohydraulics revisted: palaeoslope estimation in coarse-grained braided rivers. Basin Res., 8, 243-254, 1996.

Parker, G., Self-formed straight rivers with equilibrium banks and mobile bed. Part 2. The gravel river, J. Fluid Mech., 89, 127-146, 1978. doi:10.1017/S002112078002505.

Pettijohn, F.J., Sedimentary rocks, Harper and Brothers, New York, 718 pp., 1957.

Pfeiffer, A.M., Finnegan, N.J., and Willenbring, J.K., Sediment supply controls equilibrium channel geometry in gravel rivers, Proc. Natl. Acad. Sci. U.S.A., 114, 3346-3351, 2017.

Philips, C.B., and Jerolmack, D.J., Self-organization of river channels as a critical filter on climate signals, Science, 352, 649-697, 2016.

Potsma, G., and Roep, T., Resedimented conglomerates in the bottomsets of Gilbert-type gravel deltas, J. Sed. Petrol., 55, 874-885, 1985.

Powell, M.D., Ockleford, A., Rice, S.P., Hillier, J.K., Nguyen, T., Reid, I., Tate, N.J., and Ackerley, D., Structural properties of mobile armors formed at different flow strengths in gravel-bed rivers. J. Gephys. Res. – Earth Surface; 121, 1494-1515, 2016.

Qin, J., Zhong, D., Wang, G., and Ng, S.L., Influence of particle shape on surface roughness: Dissimilar morphological structures formed by man-made and natural gravels, Geomorphology, 190, 16-26, 2013.

Rust, B.R., Depositional models for braided alluvium, in: Fluvial sedimentology, edited by: Miall, A.D., Mem. Can. Soc. Petrol. Geol., 5, 221-245, 1978.

Rust, B.R., Proximal braidplain deposits in the Middle Devonian Malbaie Formaiton of eastern Gaspé, Quebec, Canada, Sedimentology, 31, 675-695, 1984.

Rust, B.R., and Gostin, V.A., Fossil transverse ribs in Holocene alluvial fan deposits, Depot Creek, South Australia, J. Sediment. Petrol., 51, 441-444, 1981.

Sengupta, S., Studies on orientation and imbrication of pebbles with respect to cross-stratification, J. Sed. Petrol., 36, 227-237, 1966.

Shao, Z., Zhong, J., Li, Y., Mao, C., Liu, S., Ni, L., Tian, Y., Cui, X., Liu, Y., Wang, X., Li, W., and Lin, G., Characteristics and sedimentary processes of lamina-controlled sand-particle imbricate structure in deposits of Lingshan Island, Qingdao, China, Sci. China Earth Sci., 57, 1061-1076, 2014.

Schlunegger, F., Burbank, D.W., Matter, A., Engesser, B., and Mödden, C., Magnetostratigraphic calibration of the Oligocene to Middle Miocene (30-15 Ma) mammal bizones and depositional sequences of the central Swiss Molasse basin, Eclogae geol. Helv., 89, 753-788, 1996.

Schlunegger, F., Jordan, T.E., and Klaper, E.M., Controls of erosional denudation in the orogeny on foreland basin evolution: The Oligocene central Swiss Molasse Basin as an example, Tectonics, 16, 823-840, 1997.

Schlunegger, F., and Norton, K.P., Climate vs. tectonics: the competing roles of Late Oligocene warming and Alpine orogenesis in constructing alluvial megafan sequences in the North Alpine foreland basin, Basin Res., 27, 230-245, 2015.

Schlunegger, F., Norton, K.P., Delunel, R., Ehlers, T.A., and Madella, A., Late Miocene increase in precipitation in the Western Cordillera of the Andes between 18-19°

latitudes inferred from shifts in sedimentation patterns, Earth Planet. Sci. Lett., 462, 157-168, 2017.

Schlunegger, F. and Castelltort, S., Immediate and delayed signal of slab breakoff in Oligo/Micoene Molasse deposits from the European Alps, Sci. Rep. 6, 31010, 2016.

Shaw, J, and Kellerhals, R., Paleohydraulic interpretation of antidune bedforms with applications to antidunes in gravel, J. Sediment. Petrol., 47, 257-266, 1977.

Shields, A., Andwendungen der Aehnlichkeitsmechanik und der Turbulenzforschung auf die Geschiebebewegung. Mitt. Preuss. Versuch. Wasserbau Schiffbau, 26, Berlin, 1936.

Simons, E.V., and Richardson, E.V., Discussion of resistance properties of sediment-laden streams, Am. Soc. Civil Eng. Trans., 125, 1170-1172, 1960.

Sinclair, H.D., and Jaffey, N., Sedimentology of the Indus Group, Ladakh, northern India: implications for the timing of initiation of the paaeo-Indus River. J. Geol. Soc. London, 158, 151-162, 2001.

Slootman, A., Simpson, G., Castelltort, S., and De Boer, P.L., Geological record of marine tsunami backwash: The role of the hydraulic jump, Depositional Record, 1-19, 2018.

Spicher, A., Geologische Karte der Schweiz 1:500’000, Schweiz. Natf. Ges., 1980.

Spreafico, M., Hodel, H.P., and Kaspar, H., Rauheiten in ausgesuchten schweizerischen Fliessgewässern, Berichte des BWG, Seri Wasser, 102 p., Bern, 2001.

Stürm, B., Die Rigischüttung. Sedimentpetrographie, Sedimen tologie, Paläogeographie, Tektonik, PhD thesis, Univ. Zürich, Switzerland, 98 p., 1973.

Van der Berg, F., and Schlunegger, F., Alluvial cover dynamics in response to floods of various magnitudes: The effect of the release of glaciogenic material in a Swiss Alpine catchment, Geomorphology, 141, 121-133, 2012.

Wickert, A.D., and Schildgen, T.F., Long-profile evolution of transport-limited gravel-bed rivers, Earth Surf. Dynam. Discuss., doi: org/10.5194/esurf-2018-39.

Wong, M., and Parker, G., Reanalysis and correction of bed-load relation of Meyer-Peter and Müller using their own database, J. Hydraul. Eng., 132, 1159-1168, 2006.

Taki, K., and Parker, G., Transportational cyclic steps cre- ated by flow over an erodible bed. Part 1. Experiments, J. Hydrol. Res., 43, 488–501, 2005.

Todd, S.P., Process deduction from fluvial sedimentary structures, in: Advances in fluvial dynamics and stratigraphy, edited by: Carling, P.A., and Dawson, M.R., John Wiley & Sons Ltd, 299-350, 1996.

Trieste, D.J., Evaluation of supercritical/subcritical flows in high-gradient channel, J. Hydr. Eng., 118, 1107-1118, 1992.

Trieste, D.J., Supercritical flows versus subcritical flows in natural channels, in: Hydraulic Engineering '94: Proceedings of the 1994 Conference of the Hydraulics Division, edited by: Cotroneo, G.V., and Rumer, R.R., Am. Soc. Civ. Eng., New York, 732-736, 1994.

Tucker, G., and Slingerland, R., Drainage basin responses to climate change, Water Resour. Res., 33, 2031-2047, 1997.

Whipple, K.X., Bedrock rivers and the geomorphology of active orogens, Ann. Rev. Earth Planet. Sci., 32, 151–185, 2004.

Wiberg, P.L., and Smith, J.D., Velocity distribution and bed roughness in high-gradient streams, Water Resour. Res., 27, 825-838, 1991.

Yagishita, K., Paleocurrent and fabric analyses of fluvial conglomerates of the Paeogene Noda Group, northeast Japan, Sed. Geol., 109, 53-71, 1997.

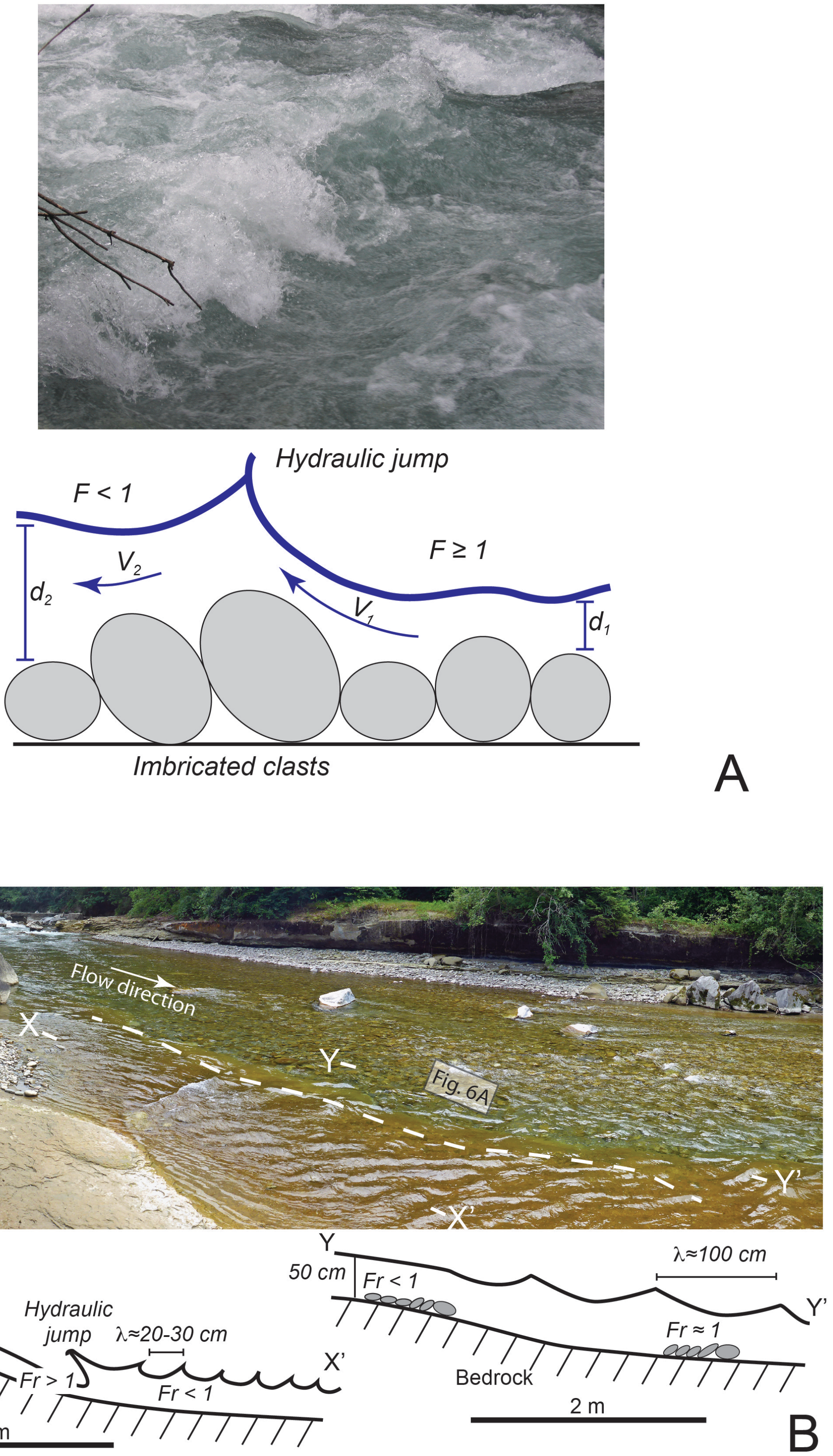

Figure 1

Figure 1

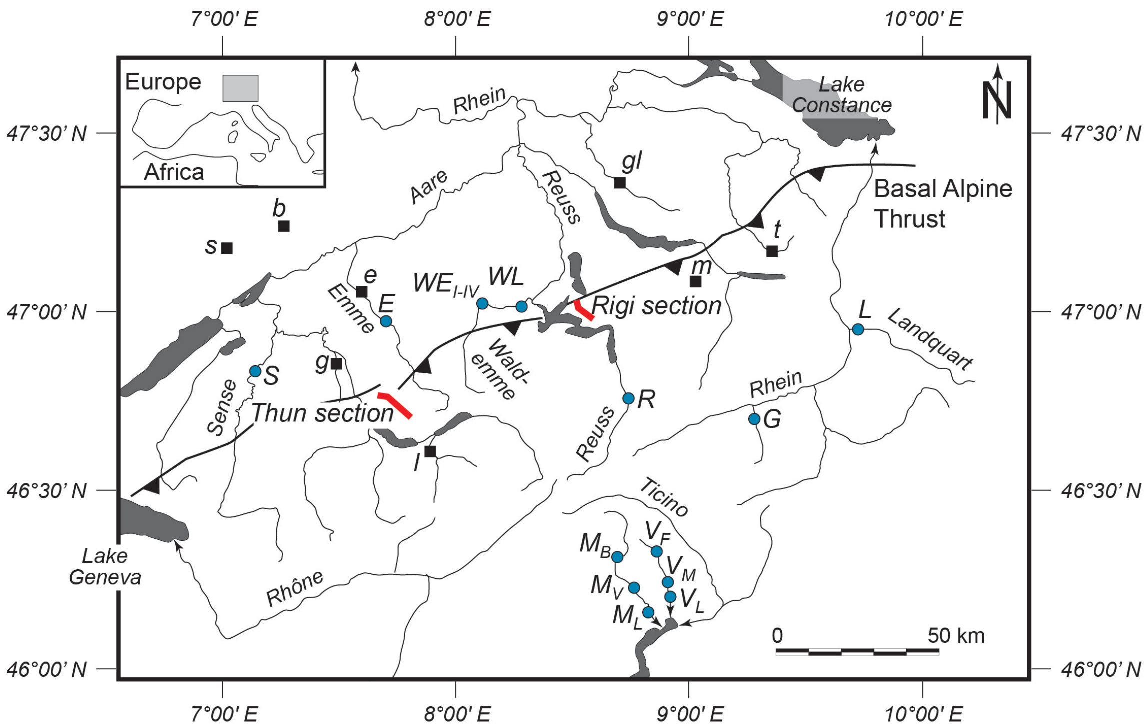

Figure 2

Figure 2

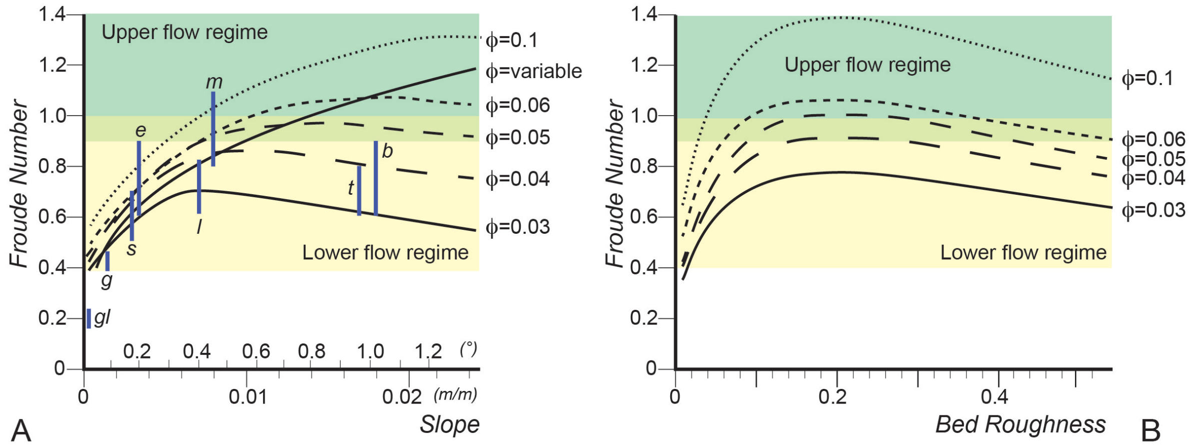

Figure 3

Figure 3

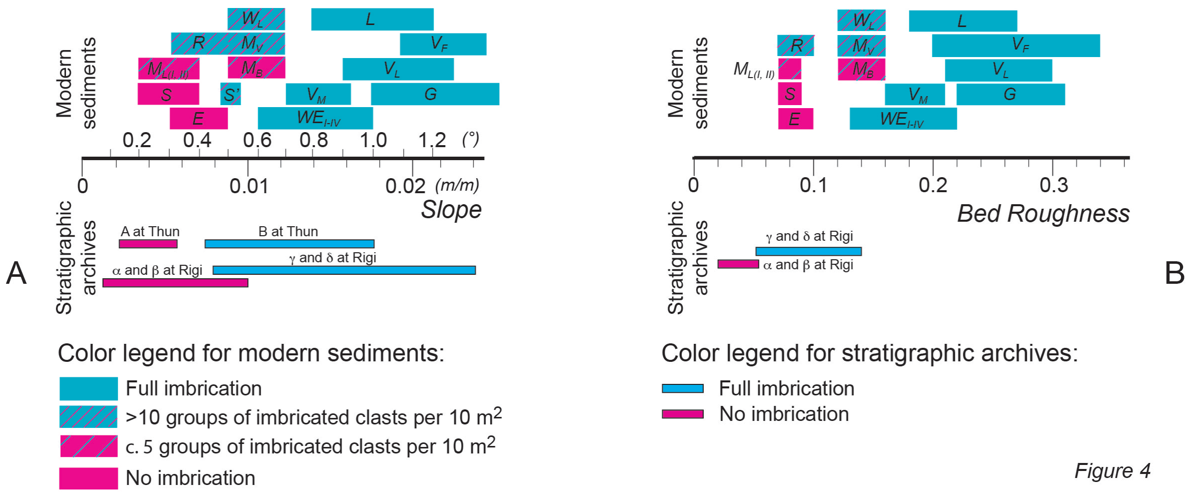
A
B
Modern sediments
Stratigraphic archives
0.2 0.4 0.6 0.8 1.0 1.2 (°)
0 0.01 0.02 (m/m)
Slope
A at Thun
B at Thun
γ and δ at Rigi
α and β at Rigi
0 0.1 0.2 0.3
Bed Roughness
Color legend for modern sediments:
Full imbrication
>10 groups of imbricated clasts per 10 m2
c. 5 groups of imbricated clasts per 10 m2
No imbrication
Color legend for stratigraphic archives:
Full imbrication
No imbrication
Figure 4

Figure 4

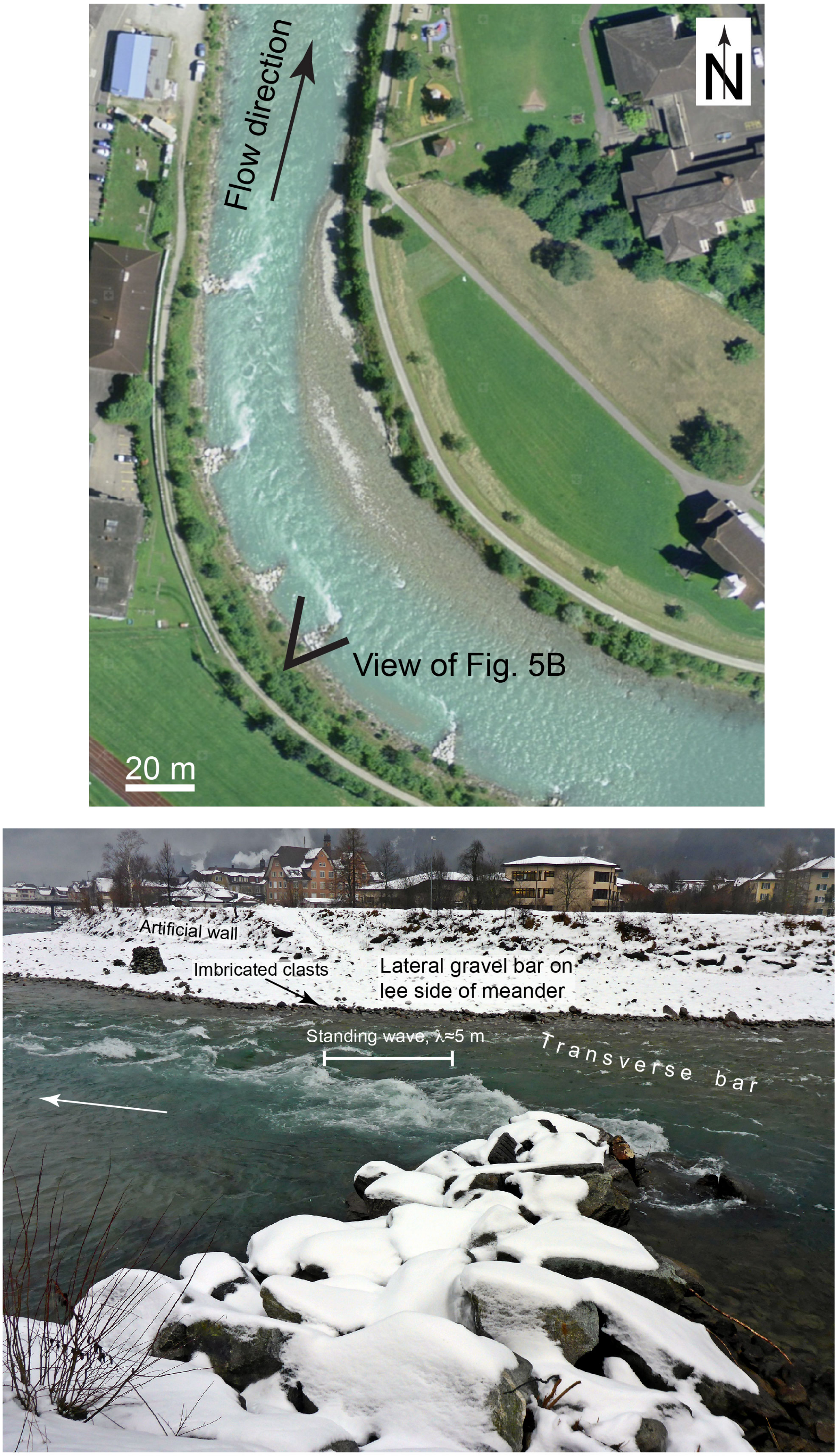
Flow direction
N
View of Fig. 5B
20 m
Artificial wall
Imbricated clasts
Lateral gravel bar on
lee side of meander
Standing wave, λ≈5 m
Transverse bar

A

B

Figure 5

Figure 6

Figure 6

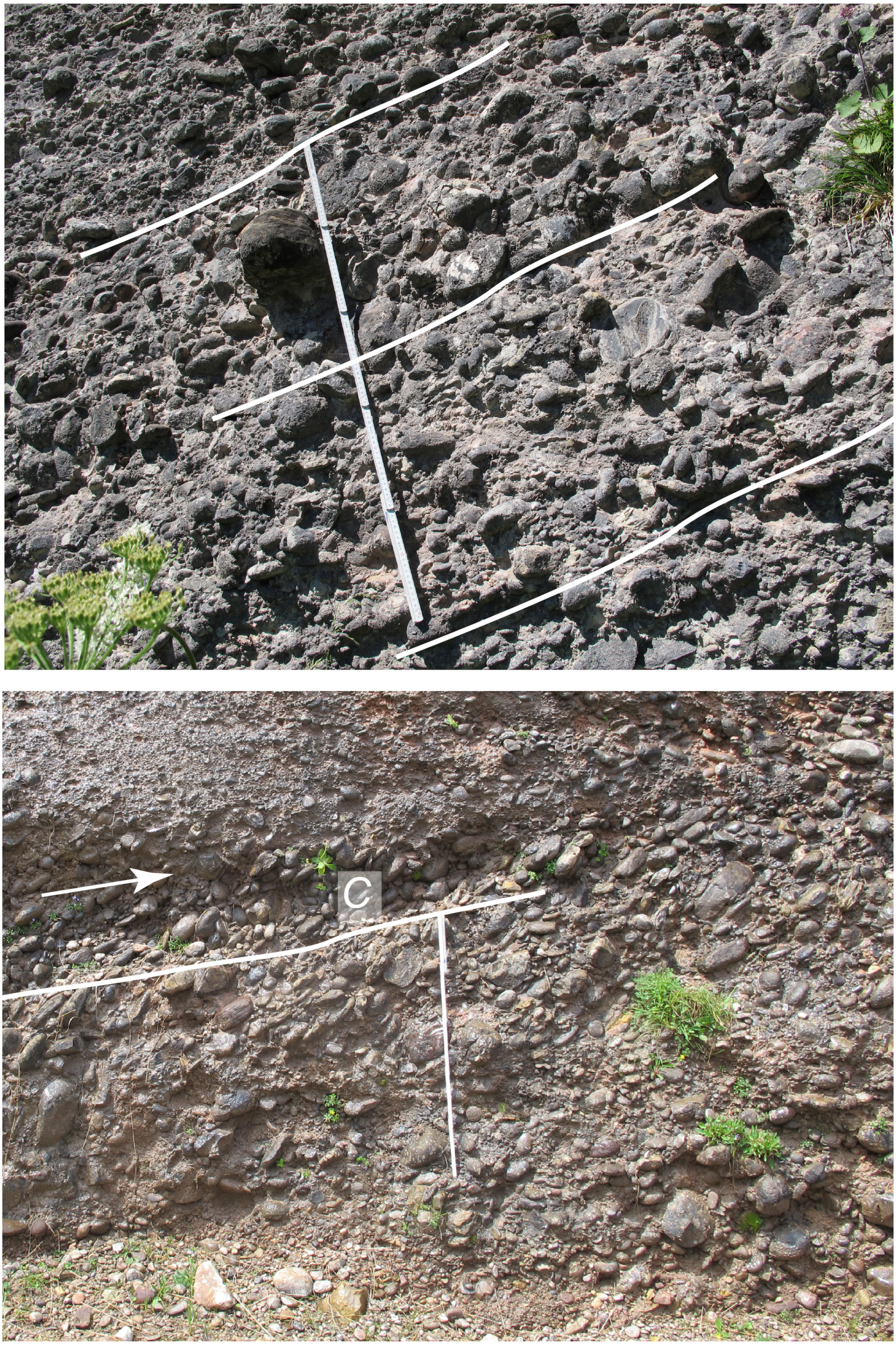

A
B

Figure 7

Figure 7

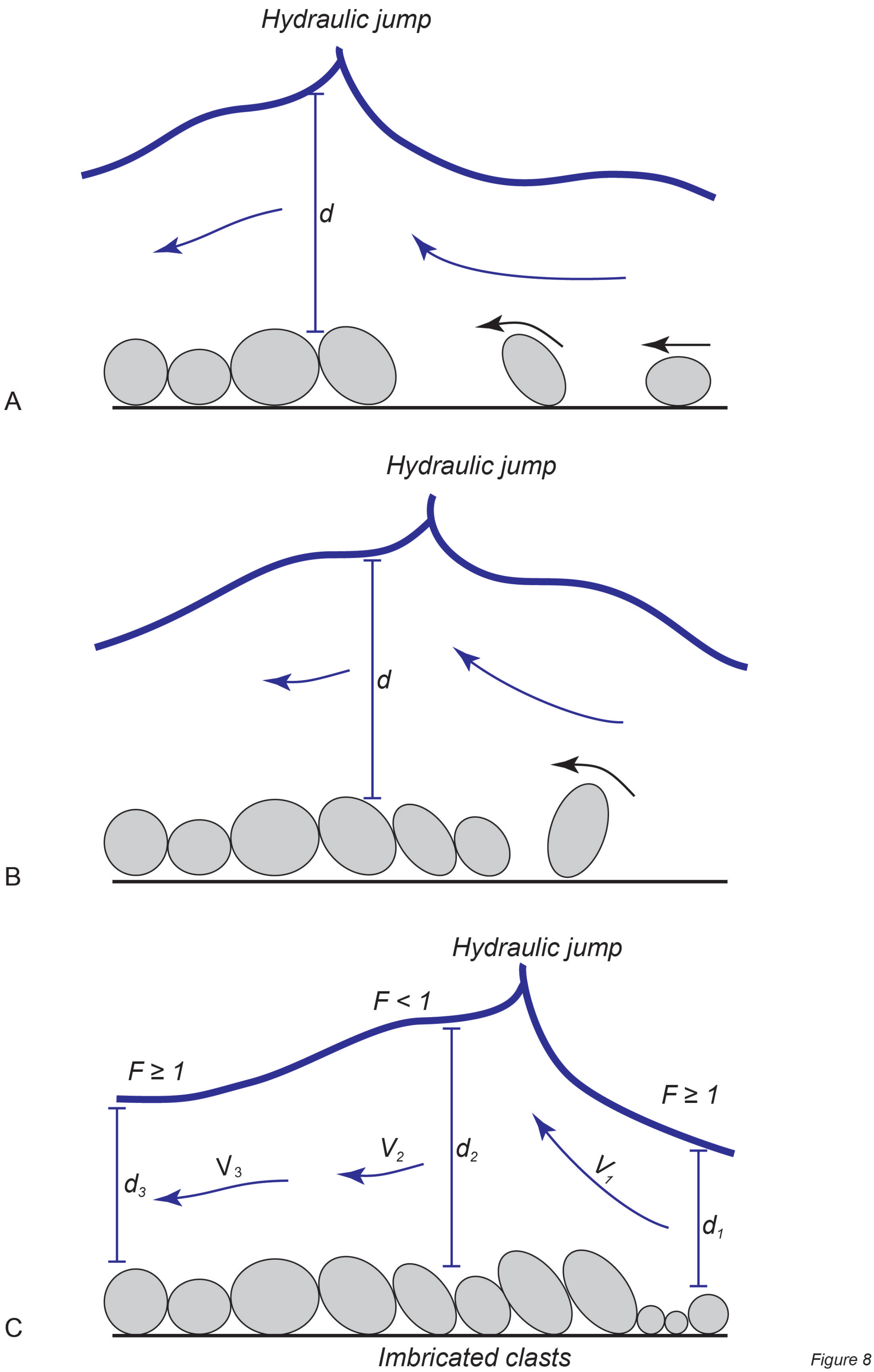

1135

1136 Figure 8

Modern gravel bars

Site name	*Abbreviation*	*Site coordinates*	*D84 (cm)*	*D50 (cm)*	*D84/D50*	*D96 (cm)*	*Gradient (m/m)*	*Gradient (°)*	*Inferred water depth d (m)*	*Roughness*	*Imbrication*
Emme	E	46°57'08N / 7°44'59E	2.3	0.9	2.56	5.2	0.005-0.008	0.4±0.1	0.5-0.8	0.07-0.10	mostly no
Glenner	G	46°44'42N / 9°13'04E	12	2.88	4.17	27.4	0.017-0.024	1.2±0.2	0.4-0.6	0.22-0.31	mostly yes; largest boulders imbricated; smaller pebbles deposited in-between without preferred orientation, sand covers the clast fabric
Landquart	L	46°57'08N / 7°44'59E	10	2.5	4.00	13.5	0.014-0.021	1.0±0.2	0.4-0.6	0.18-0.27	yes
Maggia Bignasco	MB	46°44'42N / 9°13'04E	2.7	0.85	3.18	13	0.009-0.012	0.6±0.1	0.2	0.12-0.16	mostly no, but triplets of imbracted clasts occur in places as inferred from photos
Maggia Visletto	MV	46°58'26N / 9°36'29E	9.5	2.29	4.15	20	0.009-0.012	0.6±0.1	0.3-0.5	0.12-0.16	partly yes
Maggia Losone I	ML I	46°20'08N / 8°36'25E	4	0.79	5.06	14	0.005-0.007	0.3±0.1	0.5-0.6	0.07-0.09	triplets and quadruplets of imbricated clasts occur in places
Maggia Losone II	ML II	46°18'30N / 8°36'35E	6	1.12	5.36	12.65	0.005-0.007	0.3±0.1	0.7-1.0	0.07-0.09	triplets and quadruplets of imbricated clasts occur in places
Verzasca Frasco	VF	46°10'46N / 8°45'33E	2.5	0.75	3.33	7	0.015-0.026	1.3±0.2	0.1	0.20-0.34	imbricated
Verzsca Motta	VM	46°10'15N / 8°46'10E	4.3	1.44	2.99	18.75	0.012-0.016	0.9±0.2	0.2-0.3	0.16-0.21	largest boulders imbricated smaller pebbles deposited in-between withour preferred orientation, finer-grained bedforms show imbricated clasts where no boulders are present
Verzasca Lavartezzo	LV	46°20'20N / 8°48'03E	5	1.3	3.85	30	0.016-0.023	1.1±0.2	0.2-0.3	0.21-0.30	largest boulders imbricated smaller pebbles deposited in-between without orientation as inferred from photos
Reuss		46°16'28N / 8°48'34E	3.2	0.88	3.64	6.37	0.005-0.008	0.4±0.1	0.3-0.5	0.07-0.10	to large extents yes,triplets and quadruplets of imbricated clasts occur in places. Stream shows standing waves and hydraulic jumps in steep reaches and lower flow regime conditions in flat segments
Sense		46°15'21N / 8°50'23E	6	2.42	2.48	9.58	0.005-0.007	0.3±0.1	0.7-1.0	0.07-0.09	mostly no; imbrications only at the steep downstream slip faces of transerves bars
Waldemme Littau	WL	46°48'53N / 8°39'16E	3.5	0.9	3.89	8.36	0.009-0.012	0.6±0.1	0.2-0.3	0.12-0.16	triplets and quadruplets of imbricated clasts occur in places
Waldemme Entlebuch I	WE I	46°53'20N / 7°20'56E	3	1	3.00	9	0.01-0.017	0.8±0.2	0.1-0.2	0.13-0.22	yes
Waldemme Entlebuch II	WE II	47°03'04N / 8°15'13E	8	2.43	3.29	18	0.01-0.017	0.8±0.2	0.4-0.6	0.13-0.22	yes
Waldemme Entlebuch III	WE III	47°01'57N / 8°04'03E	5.7	2.57	2.22	14	0.01-0.017	0.8±0.2	0.3-0.5	0.13-0.22	yes
Waldemme Entlebuch IV	WE IV	47°01'57N / 8°04'03E	8.2	2.68	3.06	18	0.01-0.017	0.8±0.2	0.4-0.7	0.13-0.22	yes

Stratigraphic archives

Rigi conglomerates

Segment	*D84 (m)*	*Slope (m/m)*	*Slope (°)*	*Inferred water depth d (m)*	*D84/d*	*Imbrication*
δ	0.07-0.12	0.009-0.027	0.9±0.4	1.2±0.35	0.05-0.14	yes, in places
γ	0.06-0.1	0.008-0.015	0.65±0.2	1.2±0.4	0.04-0.12	partly yes
β	0.04-0.06	0.005-0.01	0.4±0.2	1.7±0.5	0.02-0.05	no
α	0.04-0.06	0.002-0.005	0.2±0.06	2.5±0.8	0.02-0.04	no

Thun conglomerates

Unit	*D84 (m)*	*Slope (m/m)*	*Slope (°)*	*Inferred water depth d (m)*	*D84/d*	*Imbrication*
B	not availble	0.008-0.017	0.72±0.3	1.5-3	not availble	yes, in places
A	not available	0.003-0.005	0.23±0.1	3-5	not availble	no

Table 1